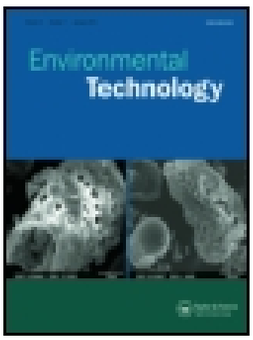

Environmental Technology

ISSN: (Print) (Online) Journal homepage: https://www.tandfonline.com/loi/tent20

Eco-friendly approach for efficient catalytic degradation of organic dyes through peroxymonosulfate activated with pistachio shell-derived biochar and activated carbon

Ali Gholami & Fakhreddin Mousavinia

To cite this article: Ali Gholami & Fakhreddin Mousavinia (2021): Eco-friendly approach for efficient catalytic degradation of organic dyes through peroxymonosulfate activated with pistachio shell-derived biochar and activated carbon, Environmental Technology, DOI: 10.1080/09593330.2021.1922510

To link to this article: https://doi.org/10.1080/09593330.2021.1922510

Published online: 17 May 2021.

ENVIRONMENTAL TECHNOLOGY
https://doi.org/10.1080/09593330.2021.1922510

Eco-friendly approach for efficient catalytic degradation of organic dyes through peroxymonosulfate activated with pistachio shell-derived biochar and activated carbon

Ali Gholami and Fakhreddin Mousavinia

Faculty of Chemistry, Department of Analytical Chemistry, University of Kashan, Kasha, Iran

ABSTRACT

This study introduces a simple method for the preparation of biochar (BCP) and activated carbon using pistachio (ACP) external hull as residual solid waste. Low-cost raw materials, biodegradable, recyclable and organic solid wastes are advantages of this method. Furthermore, complete degradation of methyl orange (MO) and methylene blue (MB) to H_2O and CO_2 as eco-friendly compounds in mild reaction condition occurs at a short time**.** Also, the effects of crucial parameters (temperature, time, catalyst dosage, initial dye and oxidant concentration, initial reaction pH level and radical scavengers), capability, adaptability, performance and reusability of ACP were also evaluated. The results displayed that dyes could be decomposed effectively by the PMS/ACP-800 system. Furthermore, the sulphate radical ($SO_4^{\bullet -}$) was a major active role in the degradation process, while hydroxyl radical ($^{\bullet}OH$) played a minor role. Overall, ACP had yielded high degradation of MB and MO dyes; therefore, ACP-800 could be effectively and reliably applied in the treatment of industry effluents containing MB and MO dyes.

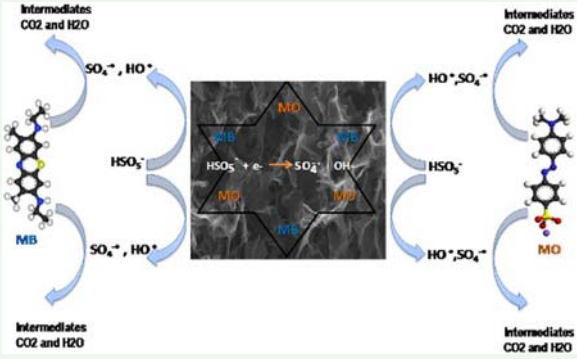

ARTICLE HISTORY
Received 17 January 2021
Accepted 19 April 2021

KEYWORDS
Pistachio shell; degradation; methylene blue; methyl orange; peroxymonosulfate

1. Introduction

Synthetic dyes are being used widely in leather, textile, paint, paper, plastic, cosmetics, printing, food and pharmaceutical industries and the like. In recent times, there has been an increasing concern about synthetic dyes that are released into waste water in environment and usually are stable for an extended time due to their non-biodegradable nature [1,2]. Most of these dyes in waste water are considered toxic, carcinogenic and mutagenic and consequently, exposure to them is much harmful to the ecosystem. They can cause numerous problems such as skin irritation, dermatitis and rashes, liver and kidney damage, headaches, diarrhoea, nausea, joint pain, irregular heartbeat, seizures and poisoning the central nervous system in both humans and animals [3–5]. Therefore, owing to the biotoxicity and constancy in structures of these organic dyes, it is highly necessary to develop eco-friendly methods for the reduction or removal of dyes and dyestuffs in waste water.

Diverse physicochemical methods have been extensively applied including the adsorption [7–15], flocculation [16], coagulation [17,18], membrane separation or filtration [19–21], chemical oxidation [22–24], catalytic degradation [25–29], photo catalytic degradation [30–36], electrochemical decomposition [37], ozonation [38] and Fenton process [39–41] to treat the waste waters contaminated with dyes [6].

Lately, advanced oxidation processes (AOPs) have been proposed to treat the emerging contaminants in

CONTACT Ali Gholami AGholami@kashanu.ac.ir Faculty of Chemistry, Department of Analytical Chemistry, University of Kashan, Kashan, I.R 8731753153, Iran

the water samples. The conventional AOPs show excellent performance in the removal of emerging contaminants, and their mechanisms are chiefly based on the hydroxyl and sulphate anion radicals that are generated via peroxymonosulfate (PMS) reactions in the solution [42].

In recent years, advanced degradation processes based on carbon have been widely studied and become a prospective method for the destruction of Methyl Orange (MO) and Methylene Blue (MB) as main waste water-contaminating components, which are used in million tons annually [8,10,26,37,39,43–45]. Among these, the following can be mentioned to the degradation of MO; under microwave irradiation using Fe/Fe_3C@C catalysts through generations of $OH^{\bullet}$ and $O_2^{\bullet-}$ free radicals [43], carbon-doped BiOI photocatalysts [45] and carbon foam-loaded nano-TiO photocatalyst [44] and also degradation of MB; by CoO loaded on mesoporous carbon nitride through the formation of $SO_4^{\bullet-}$ and $OH^{\bullet}$ as major reactive species [26] and by N-doped carbon/CuO-Fe2O3 (NC-CuFe) nanocomposite in the presence of H_2O_2 [39]. On the other hand, in most above-mentioned studies, MO and MB are only decomposed into smaller substances that may still cause harm to the environment. Among carbon-based catalysts or absorbents, activated carbons, due to their user-friendliness, high specific area and good performance in removal dyes, have attracted the attention of researchers [8–11] but several difficulties, such as low removal efficiency, requirements of costly reagents and sophisticated monitoring system and disposal problem of toxic sludge, limit their application. Therefore, developing low-cost raw materials for the preparation of activated carbon would be more desirable. Carbonaceous materials, as environment-friendly catalysts, reduce the use of the other types of oxidant activators such as toxic and expensive metals.

The huge amount of crop wastes is a serious global problem. Consequently, extensive studies have been performed to apply these solid wastes [46–48]. Especially, pistachio has attracted more attention due to its massive total world production (around 586,200 MT in 2017–2018 [49,50]).

On the other hand, one of the most important horticultural crops cultivated in Iran is pistachio. According to the published statistics, the area under cultivation of pistachio in Iran is more than 300,000 ha. Currently, Iran is the largest producer of pistachios in the world and annually, disposal of the wastes obtained from cultivation and processing is an important problem [51]. Pistachio's external green hull is 35–45 % of its total weight that is generally dumped as by-products and solid waste [50], by the agricultural and food industries. Several studies have been done on pistachio to use it as a renewable source such as adsorption of Cu(II) using pistachio shell as a green absorbent [52], extraction of polysaccharides from pistachio external hull as a meat preservative in food products [50], stabilizing Pickering emulsions by cellulose nanocrystals are produced by pistachio shells, removal of uranium from contaminated industrial seawater is done using pistachio shells [53,54]. It seems that pistachio residual is a suitable resource for the production of activated carbon [55].

Pistachio shell mostly consists of lignin, hemicelluloses and cellulose. Such a composition makes pistachio shell a suitable raw material to produce new adsorbents and catalysts for waste water treatment systems [56]. Keeping all these in view, this study focuses on the production of activated carbon using pistachio solid waste as a renewable source through a simple process with potassium oxalate as the activating reagent. Potassium hydroxide is the most widely used activating reagent, but due to toxicity and high corrosiveness, its application for high-scale production is restricted. Potassium oxalate is preferred for producing active carbons with different applications. An additional benefit of this activating agent is it produces high surface area and, importantly, the product yield is almost twice that of using the KOH activator [57–59].

Therefore, in this study, the less corrosive and easy controllable potassium oxalate salt was used as an alternative reagent to produce biochar and activated carbon from pistachio nut shell. The efficacy of the produced activated carbon and PMS reagent as an effective and reusable catalyst system was studied in complete degradation of MO and MB to H_2O and CO_2.

2. Material and methods

2.1. Material and apparatus

All chemicals were at least of analytical grade and were used as received without further purification. PMS (potassium proxymonosulfate, as oxone $KHSO_5{\cdot}0.5KHSO_4$ $0.5K_2SO_4$, $KHSO_5 \geq 47\%$) and tert-butyl alcohol were purchased from Sigma-Aldrich. Methylene blue (MB, $C_{16}H_{18}ClN_3S$. x H_2O ($x = 2$ or 3)), methyl orange (MO, $C_{14}H_{14}N_3NaO_3S$), potassium oxalate mono hydrate ($C_2K_2O_4.H_2O$), sodium hydroxide (NaOH), hydrochloric acid (HCl) and ethanol (ETOH) were purchased from Merck. TOC reagent was purchased from HACH Company. A seven compact pH meter (Mettler Toledo, S220) was

used to measure the pH values. Ultrapure water (18.2 MΩ·cm) from an AquaMax – Basic 360 Series water purification system was used to prepare all the solutions required in the present work. A shimadzu analytical balance (AUW 220 D series) was used for weighing the dyes and PMS. Electric muffle furnace (ADVANTEC-FUW232PA) and electric drying oven (ADVANTEC – DRA430DA) were used for preparing the pistachio nut shell catalysts and drying of the catalysts in the preparation step, respectively. The IR spectra (KBr) were recorded on Perkin – Elmer GX Fourier transform infrared spectrometer (FT-IR). The XRD measurements were done by a Bruker D8 Advance powder diffractometer, using Cu K_α (λ = 1.54 A°) as the incident radiation. The GC/MS from AGILENT Company (7890A GC SYSTEM / 5975C inert MSD with triple axis detector) was applied for degradation analysis, which is equipped with the Rtx-wax polar column (USA) with a length of 30 meters, an ID of 0.25 mm and a thickness of 0.25 µm.

2.2. Preparation of the biochar and activated carbon from pistachio nut shells (BCP, ACP)

Different biochar and activated carbon were prepared by varying the temperature (500or 800°) and different ratio of pistachio nut shells (PNs) to potassium oxalate ($C_2K_2O_4$) and tested in the decolourization of MO and MB.

The crushed pistachio nut shells were dried in the oven at 100°C for one hour, after that they were pounded in the mortar by gentle blows to be converted into millimetre particles. Different ratio amounts of PNs/$C_2K_2O_4$ (W/W: 1/1, 1/1.5 and 1/2) were mixed in the crucible homogenously by blending with a spatula, then the crucible was placed in the furnace under nitrogen purging (100 ml/min) in desired temperatures (500 or 800°C) for 2 h. Then the mixture was cooled down to 100°C under nitrogen purging. The obtained biochar (BCP-500) and activated carbons (ACP-800) were washed with purified water separately till the pH of the washed solution reached to around 7.5, and finally the washed samples were dried at 100°C in the drying oven for 2 h.

2.3. Catalytic degradation experiment

The general degradation process was done in 100 mL conical flasks. The temperature (25°C) and pressure (1 atm) of the reacting solution were kept constant throughout the experiments. Desired amounts of oxidant (PMS) and dye (MO or MB stock solutions) were added into the reactor and pH adjustment was done using HCl and NaOH solutions. Then a certain amount of ACP/BCP was added into the reaction mixture which contained oxidant and dye. During degradation processes, the solution was stirred with a magnetic stirrer to ensure a complete mixing. At the given reaction time intervals, approximately 2.0 mL of sample was withdrawn and the dye content was determined immediately. The degradation of the MO and MB was monitored immediately by maximum absorbance at wavelengths of 464 and 664 nm, respectively. The C_t/C_0 value was used for illustrating the degradation efficiency, where C_0 is the initial MO or MB concentration, C_t is the concentration at time in the ACP/PMS system. The mineralization of MO/MB dyes was characterized by the TOC (total organic carbon) of the reaction solutions after 1 and 24 h. Every experiment was done three times and the obtained results were similar.

3. Result and discussion

3.1. Characterization and properties of the BCP and ACP catalyst

Biochar (BCP) and activated carbon (ACP) of pistachio shell as a carbonaceous material were derived from waste pistachio shell by pyrolysis at 500 and 800°C, respectively for 2 hrs in a closed crucible in the furnace [57,58,60]. The structural and morphological analysis of synthesized biochar and activated carbon of pistachio shell was done by a SEM (scanning electron microscope), EDAX (Energy-dispersive X-ray spectroscopy) and XRD (X-ray diffraction).

EDAX analysis was used for determining the composition and abundance of elements in samples. Figure 1 (A–C) shows the typical EDAX analysed for pistachio shell and ACP-800. Figure 1 illustrates that C, O, K and S atoms are the main chemical elements on the sample. Increased pyrolysis temperature (from 500 to 800°C) results in decreased total carbon amount from 85.01 to 66.21 %, increased oxygen amount from 10.37% to 13.31%. Table 1 summarises the EDAX data of biochar and activated carbon samples as BCP-500(1+1) and ACP-800(1+2), respectively. Except the preparation temperature (500°C), due to the performance and obtained surface area by BET experiment, the sample of BCP-500(1+1) is considered as biochar. Generally as an accepted definition, biochar is a carbon-rich, fine grained and porous material produced by heating organic matter at temperature not above 700°C [61].

It seems that at higher temperatures the porosity increases related to the conversion of aliphatic compound to aromatic compound [54]. In this process, increasing the activation temperature (800°C) of pistachio shell reduces the yield of the activated carbons. This is predicted because the content of volatile compounds is raised when activation temperature is

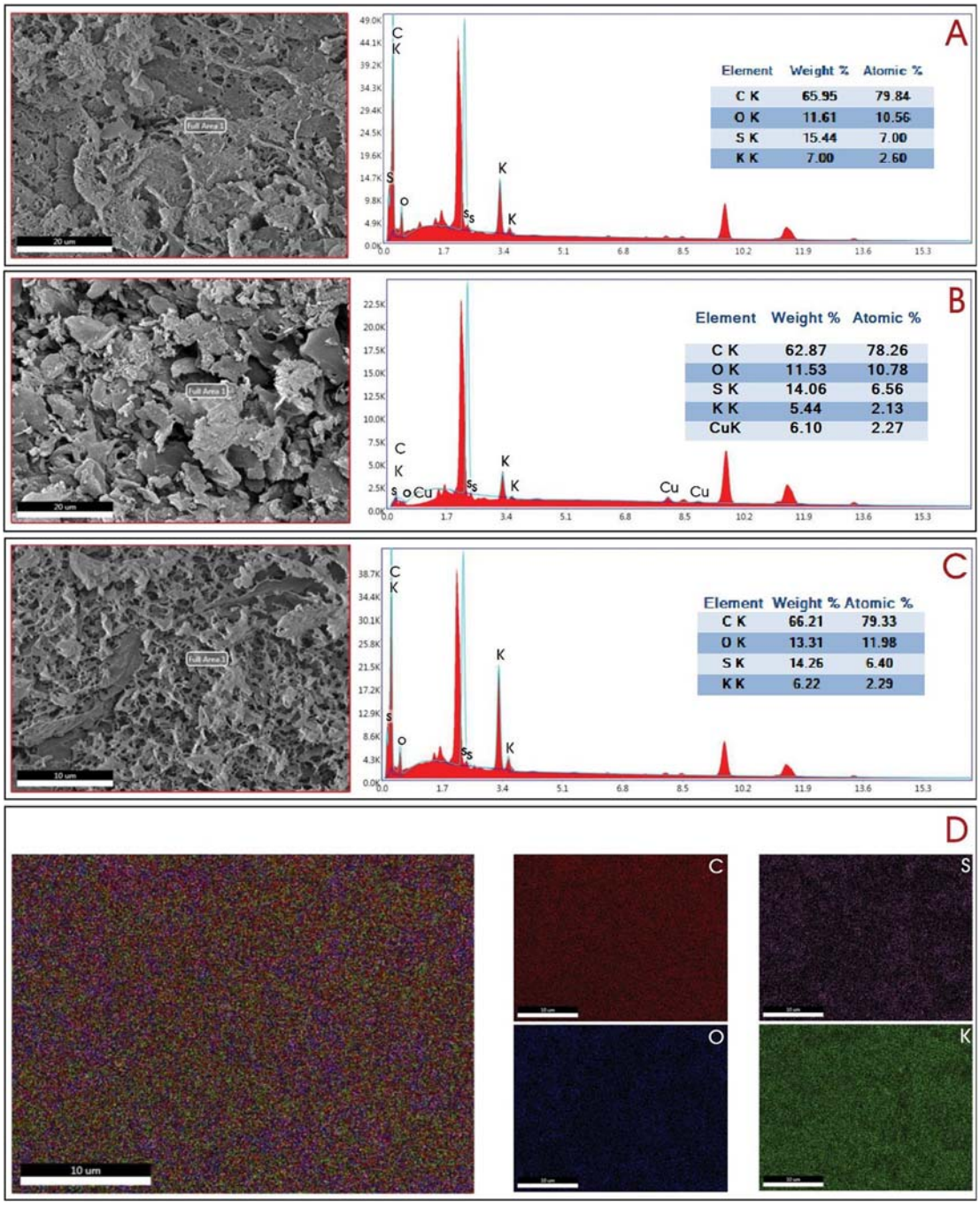

Figure 1. SEM images of (A) ACP-800(1+1), (B) ACP-800(1+1.5), (C) ACP-800(1+2), (D) EDAX pattern of ACP-800(1+2).

increased to 800°C. These are also exhibited the decrease of volatile content and increase of fixed carbon by increasing the activation temperature. The SEM image and EDAX pattern of ACP-800, prepared at various ratios of oxalate to pistachio shell, are presented in Figure 1. The surface morphology characteristics of the ACP-800, applied as a natural activator, were evaluated through SEM images. Figure 1(A–C) shows the smooth and closed surface texture of the ACP-800, and also the free space of the cavities related to the lignin, hemicellulose and cellulose of organic components [54]. There is a good possibility for oxidant and dye molecules to be trapped and degraded. In fact, the porous nature and presence of cavities on the surface of

Table 1. Elemental analysis of BCP-500(1+1) and ACP-800(1+2) obtained by the EDAX analyzer.

BCP-500(1+1)			ACP-800(1+2)		
Element	Weight%	Atomic%	Element	Weight%	Atomic%
CK	85.01	90.16	CK	66.21	79.33
OK	10.37	8.26	OK	13.31	11.98
SK	1.03	0.41	SK	14.26	6.40
KK	3.59	1.17	KK	6.22	2.29

Table 2. Textural characteristics of pistachio nut shell-derived biochars (BCP-500(1+1)) and activated carbon (ACP-800(1+2)).

Properties	Biochar (BCP-500(1+1))	Pistachio- shell-derived activated carbon (ACP-800(1+2))
BET surface area (m^2g^{-1})	114.97	1328.43
Langmuir surface area (m^2g^{-1})	137.5	1591.81
Average pore diameter (nm)	1.917	1.648
Total pore volume (cm^3g^{-1})	0.0474	0.5999

samples is useful for the trapped process for dye degradation. ACP activators applied in this investigation were produced by impregnating pistachio nut shell with a different ratio of $K_2C_2O_4.H_2O$ and then activated at 800°C. Initially, increasing the amount of $K_2C_2O_4.H_2O$ diminishes the weight loss of the activated carbon related to the inhibition of tar generation by $K_2C_2O_4.H_2O$, leading to increased carbon yield [54,62,63]. Based on the above results, the performance of ACP-800 (1+2) is presumably higher than those of ACP-800 (1+1.5) and ACP-800 (1+1).

Detailed characteristics of the porosity of char (BCP-500) and pistachio shell-derived active carbon (ACP-800(1+2)) have been summarised in Table 2. It can be observed that BET surface area, Langmuir surface area, and total pore volume of ACP-800(1+2) were improved, implying the development of additional pores during chemical activation by excess potassium oxalate at 800°C under nitrogen purging.

Figure 2 shows the XRD patterns of pistachio shell and ACP-800. Cellulose, as a main structural component in pistachio shell, is observed in the XRD patterns. In ACP-800, the intensity of the main peaks is lower and the peaks become broader confirming a less ordered structure. Furthermore, the typical peaks of the residual inorganic matter, such as K_2CO_3, are easily observed in ACP-800 due to the decomposition of $K_2C_2O_4.H_2O$ above 700°C [57].

$$K_2C_2O_4 \rightarrow K_2CO_3 + CO \quad (1)$$

$$2K_2C_2O_4 \rightarrow 2K_2CO_3 + C + CO_2 \quad (2)$$

$$K_2CO_3 + 2C \rightarrow 2K + 3CO \quad (3)$$

The XRD patterns of ACP-800 are characterized by the more or less elevated background between ($2\theta = 15$ and 45), related to the presence of organic material. The characteristic and broad peak of the carbonaceous structure can be detected. Based on the data, it is concluded that this peak is broader and weaker in ACP-800 samples, when compared to pistachio shell sample, probably implying a less ordered structure.

FT-IR spectra of biochar samples are illustrated in Figure 3. The wide peaks seen for BCP(500) at around 3442 cm^{-1} and for ACP(800) samples at around 3425 cm^{-1} indicate the presence of hydroxyl group (–OH) stretching whose intensity of peak is increased with the increment of the temperature from 500 to 800°C.

The peaks at 2855 and 2925 cm^{-1}, also observed in all samples, are attributed to aliphatic C–H deforming vibration [64,65]. Both these events occur due to the conversion of aliphatic to the aromatic structure in parallel with oxygen amount enhancement during the increase of activation temperature. The band at 1720 cm^{-1} for BCP(500) is related to ν(C=O) vibration in the carbonyl group or the presence of carboxylic bonds [66,67]. The intensity of these bands diminished at higher temperatures owing to the degradation of carbonate compounds. The bands at around 1630 $cm^{-1}$are attributed to the presence of aromatic C=O ring stretching or C=C stretching of aromatic groups in lignin which indicates the presence of residual lignin after degradation. So, these bands are more intense in the spectra obtained at higher temperatures as envisaged. It is expressed that the conjunction of the carbonyl groups with the aromatic ring is determined at the exact position of the peaks (around 1600–1700 cm^{-1}) and the proportion of these peaks is represented the charring rate [68,69]. The characteristic peaks of the aromatic C=O ring stretching appear at 1500–1430 cm^{-1}. The band at 1385 $cm^{-1}$is attributed to δ(C=H) vibration in alkanes and alkyl groups [70].

The peak shown at 1045 and 1135 cm^{-1} in biochar BCP (500) and ACP(800) are related to aliphatic ether, alcohol C –O or aromatic stretching, O–H deformation vibrations in cellulose and hemicelluloses. These functional groups decrease at temperatures higher than 300°C showing the degradation of hemicelluloses and cellulose [71,72].

In the region 800–600 cm^{-1} aromatic and hetero aromatic compounds are verified by C–H wagging vibrations. The intensity of these peaks increases for ACP(800) because of the durability of these compounds and the possible cyclization phenomenon. It is stated that the stability of biochar is dependent on the conversion of the primary carbon structure to polycyclic aromatic structures during the pyrolysis process [73].

3.2. Catalytic degradation of BCP and ACP

Figure 4(A,B) shows the decolourization of MO and MB by PMS oxidation, pistachio adsorption and pistachio

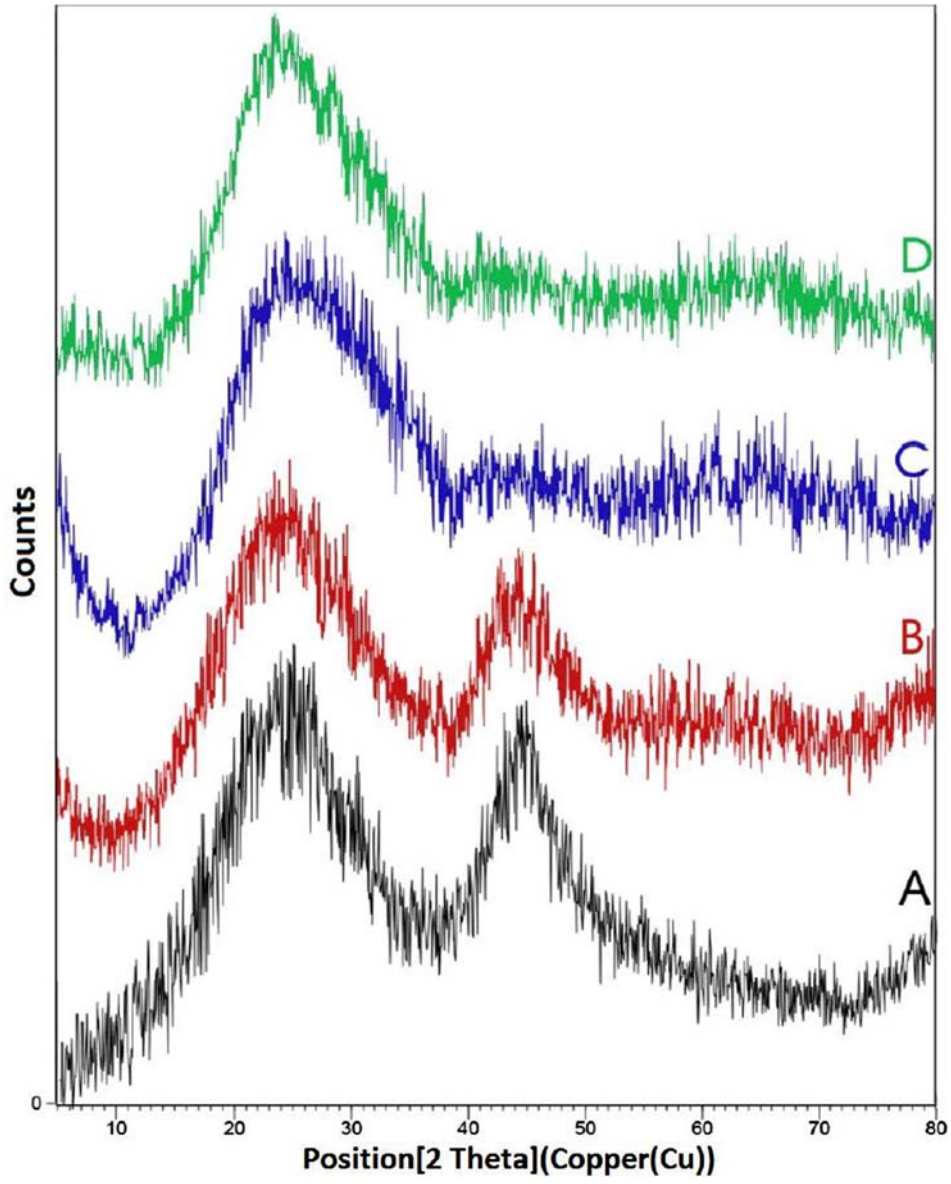

Figure 2. XRD pattern of (A) pistachio shell, (B) ACP-800(1+1), (C) ACP 800(1+1.5), (D) ACP-800(1+2).

catalytic PMS oxidation. MO and MB adsorption on the ACP activator was a fast process, and the absorption equilibrium could be reached during <10 min, as shown in Figure 4. The degradation ratios of MB and MO dyes were 27 and 23% in the system of ACP during reaction time in 90 min, respectively. It can be seen that the MB and MO elimination rates were negligible in PMS alone system related to the low oxidation potential ($E^{\circ}_{(HSO5-/HSO4-)} = +1.82$ V vs. NHE). It seems that the activation of PMS is necessary for application in degradation systems because of its low reactivity (48%). Evidently, there existed a synergistic effect in the ACP/BCP and PMS degradation systems. ACP can donate an electron to PMS to form the reactive radical and anion radical as Equations (4)–(6.) to initiate the destructive reactions [74].

$$HSO_5^- + ACP \rightarrow SO_4^{-\cdot} + OH^- + ACP^+ \quad (4)$$

$$HSO_5^- + ACP \rightarrow SO_4^{2-} + OH^{\bullet} + ACP^+ \quad (5)$$

$$HSO_5^- + ACP^+ \rightarrow SO_5^{-\bullet} + H^+ + ACP \quad (6)$$

Therefore, ACP has a great catalytic activity of PMS activation for MB and MO degradation. Furthermore, it should also be detected that the MB and MO degradation rates in the both systems are equal (Figure 4(A, B)). This phenomenon may be related to the fact that ACP and BCP had an equal adsorption rate for MB and MO dyes. These results illustrate that PMS oxidation catalysed by ACP and BCP play an essential role in

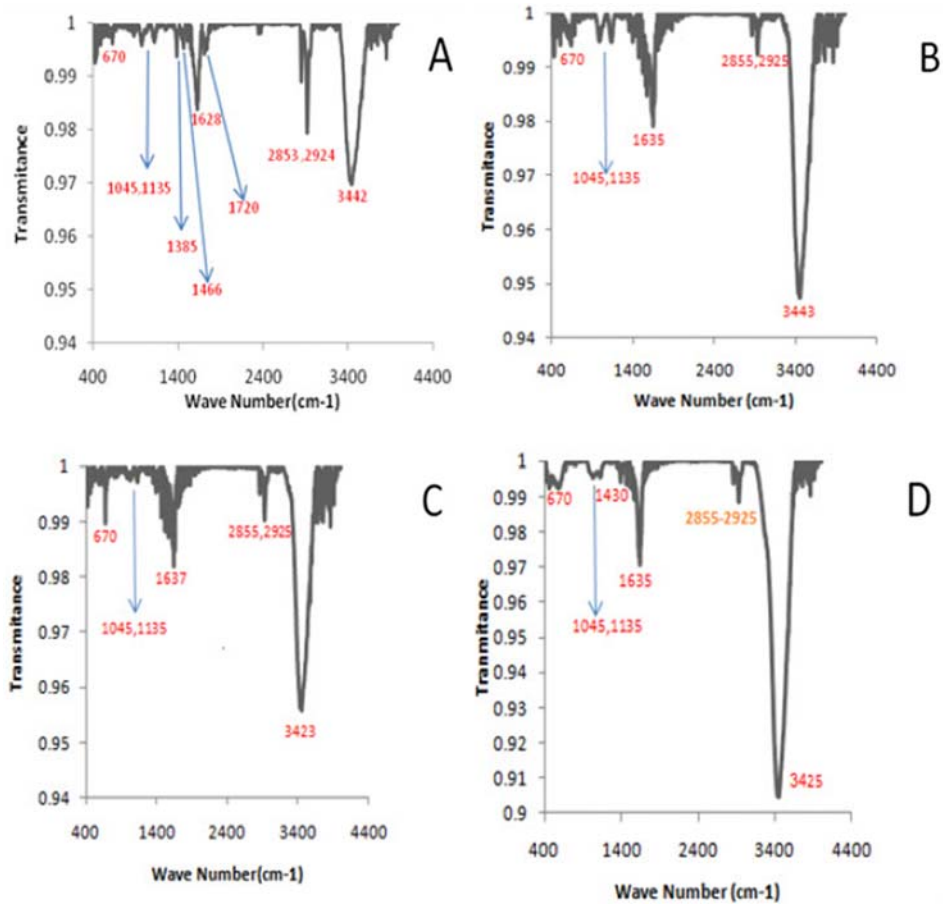

Figure 3. FTIR spectra of biochars: A: BCP500(1+1), B: ACP800(1+1), C: ACP800(1+1.5), D: ACP800(1+2).

decolourization of MO and MB dyes. The experiment results showed that the catalytic performance of the ACP activator towards oxidant activation was significantly influenced by their annealing temperature, as shown in Figure 4(C,D). In the temperature range of 500–800°C, the ACP treated at higher temperature exhibited an increased activation potential for oxidation of MO and MB [63]. The operating parameter results confirmed that ACP-800 activator had a higher adsorption ability due to its high surface areas and higher removal efficiencies of MO (average 87.3%) when compared with BCP-500 (62%) during time reaction. To obtain further insight into the effects of pivotal parameters in the degradation efficiency of MO and MB dyes, ACP-800 (1+2) was selected for the tests in the following research studies because of its excellent catalytic efficiency (94%).

3.3. Effects of pivotal parameters on the degradation efficiency of ACP-800

3.3.1. Effect of temperature

In the AOP, degradation efficiency could be influenced strongly by parameters including temperature, amount of activator, PMS dosage, concentration of dye and pH values. Figure 5(A,B) shows the influence of temperature on the degradation rate of MO and MB. It is easy to see that the degradation efficiency of MO and MB increased with temperature from 15 to 60°C. When the temperature was 60°C, MO and MB can be oxidized during reaction time in 90 min, as shown in Figure 5. Increasing the temperature has a positive effect on the chemical degradation rate of dye and increases the activating capacity of oxidant and in parallel, PAC 800 as the catalyst could work at high temperatures that indicated the structure of the catalyst is maintained at elevated temperatures. Consequently, in this work the increase of temperature accelerates the degradation efficiency of MO and MB [75–78]. However, due to the high energy required that makes heat activation inapplicable for large scales and, given that the biological temperature in the nature is 25°C and finally, due to the proper degradation performance Figure 5(A,B), the 25°C is selected to continue the research.

3.3.2. Effect of ACP dosage

Figure 6(C,D) exhibits the effect of ACP concentration on MO and MB decolourization in the ACP-

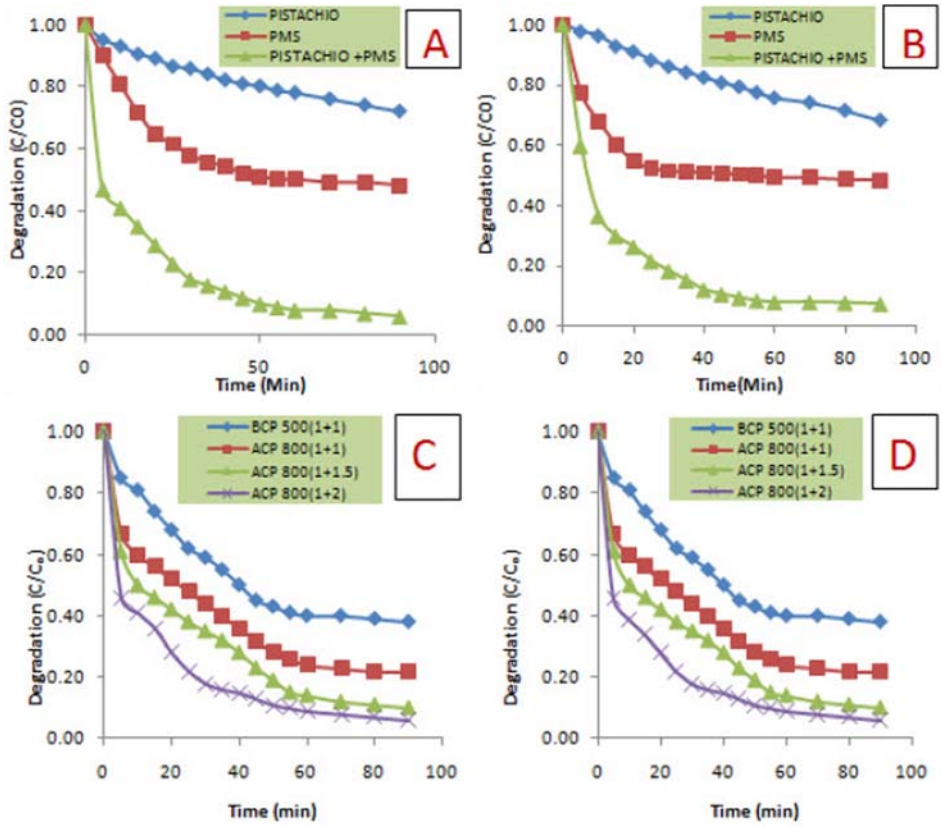

Figure 4. Effect of pivotal parameters on MO and MB degradation (A) PMS only, Pistachio only and PMS+Pistachio ($[MO]_o = 0.03$ mM (10 mg/L), [ACP] = 0.5 gr/L, $[PMS]_o = 1.6$ mM, pH = 4, 25°C), (B) PMS only, Pistachio only and PMS + Pistachio ($[MB]_o = 0.03$ mM (10 mg/L), $[ACP]_o = 0.5$ gr/L, [PMS] = 1.6 mM (25 mg/100c), Temp: 25°C), (C) Effect of BCP and ACP type on MO degradation ($[MO]_o = 0.03$ mM(10 mg/L), $[ACP]_0 = 0.5$ gr/L, [PMS] = 1.6 mM, pH = 4, 25°C), (D) Effect of BCP and ACP type on MB degradation ($[MB]_o = 0.03$ mM (10 mg/L), $[ACP]_o = 0.5$ gr/L, $[PMS]_o = 1.6$ mM, pH = 4, 25°C).

activated PMS system. The removal efficiency of MO and MB increased with the increase of ACP dosage. When the dosage of ACP was 0.1 and 0.3 g/L, respectively, the final concentration ratio (C_t/C_0) was 0.21 and 0.13 for MO, and it was 0.2 and 0.16 for MB, respectively. Moreover, a complete degradation of MO and MB was observed at last minutes when ACP dosage was 1 g/L, MO and MB was removed within 80 min. The effect of ACP on degradation was mainly due to the active sites on the surface of ACP. Higher dosage of ACP can provide more active site to adsorb and activate PMS to form radicals, which can increase the removal efficiency of MO and MB [79]. Vice versa, low dosage of ACP could not provide enough active sites to activate 1.6 mM of PMS. Accordingly, the reactive species are not enough to oxidize the dyes, resulting in the low removal efficiency of MO and MB. When the reactive species were completely consumed, the degradation of MO and MB stopped, which led to the incidence of the plateau in the curves after 80 min.

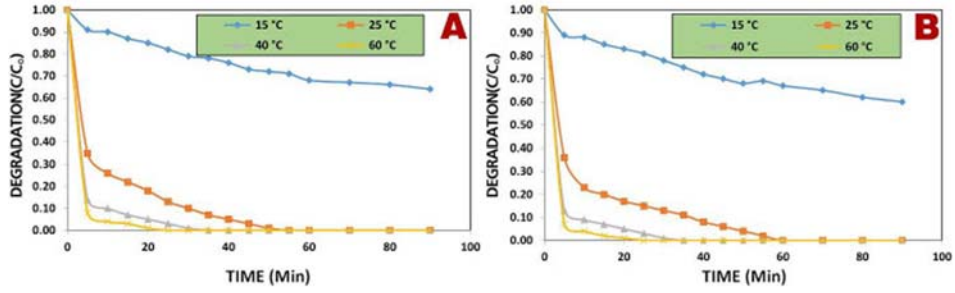

Figure 5. Effect of temperature on degradation efficiency (A) MO and (B) MB in PMS/ACP-800 (1+2).

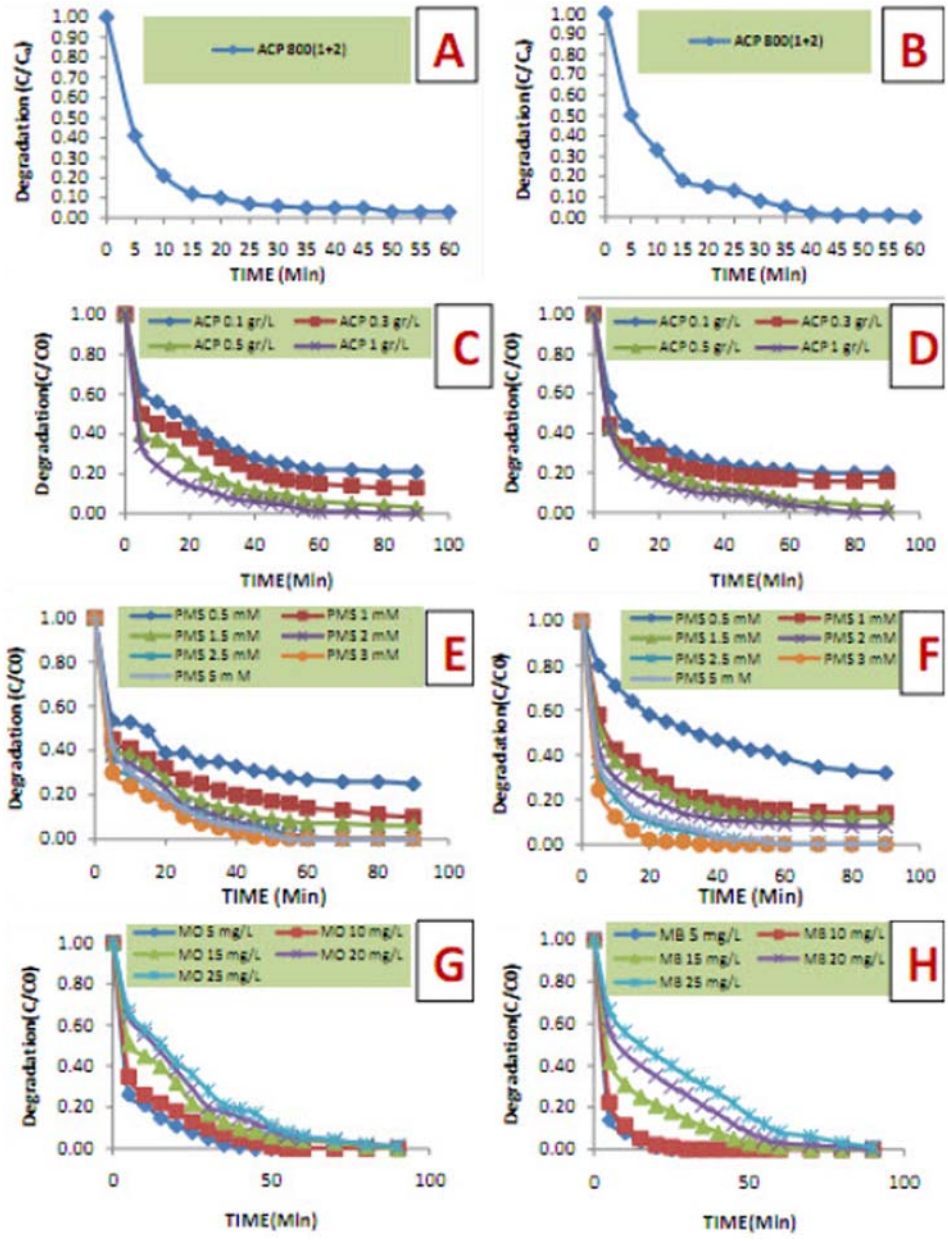

Figure 6. Effect of various parameters in the degradation of MO and MB; (**A**) Effect of time on MO degradation: $[MO]_o = 0.03$ mM (10 mg/L), $[ACP]_o = 0.5$ gr/L, $[PMS]_o = 1.6$ mM, pH = 4, 25°C, (**B**) Effect of time on MB degradation: $[MB]_o = 0.03$ mM(10 mg/L), [ACP] = 0.5 gr/L, [PMS] = 1.6 mM, pH = 3.54, 25°C, (**C**) Effect of ACP concentration on MO degradation: $[MO]_o = 0.03$ mM(10 mg/L), [ACP] = 0.5 gr/L, pH = 3.5,[PMS] = 1.6 mM, T = 25°C, (**D**) Effect of ACP concentration on MB degradation: $[MB]_o = 0.03$ mM(10 mg/L), [ACP] = 0.5 gr/L, pH = 3.5,[PMS] = 1.6 mM, T = 25°C, (**E**) Effect of PMS concentration on MO degradation: $[MO]_o = 0.03$ mM (10 mg/L), [ACP] = 0.5 gr/L, pH = 3.5, T = 25°C, (**F**) Effect of PMS concentration on MB degradation: $[MB]_o = 0.03$ mM(10 mg/L), [ACP] = 0.5 gr/L, pH = 3.5, T = 25°C,(**G**) Effect of initial MO concentration: [ACP] = 0.5 gr/L, pH = 3.5,[PMS] = 3 mM, T = 25°C, (**H**) Effect of initial MB concentration: [ACP] = 0.5 gr/L, pH = 3.5,[PMS] = 3 mM, T = 25°C.

3.3.3. Effect of PMS concentration

It can be seen that the optimal dosage of PMS was 1.0 mM for MO and MB removal efficiency. MO and MB degradation rate increased within 90 min as the PMS dosage increased from 1.0 mM, and the results are depicted in Figure 6(E,F). According to these results, it can be concluded that persistent free radicals (PFRs) formed from PMS decomposition raised with the increase of oxidant dosage. On the other hand, the content of PFRs can directly influence the degradation efficiency of dye. Although improving the PMS concentration till 3mM can accelerate the dye removal related to more oxidizing species produced, it is not an appropriate proposal to use PMS with too high dosage because of the unavoidable ecological risk of residual K^+ and $SO_4^{\bullet-}$ in the solution after application. The

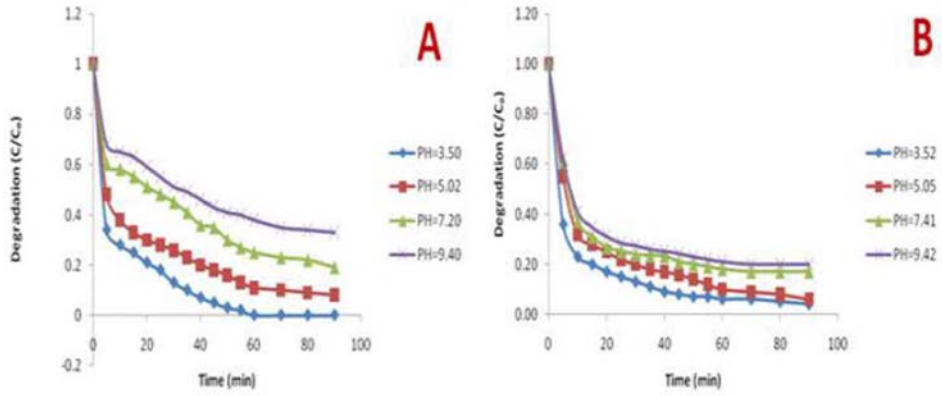

Figure 7. Effect of pH value in the degradation of MO and MB; (**A**) $[MO]_o = 0.03$ mM (10 mg/L), $[ACP]_o = 0.5$ gr/L, $[PMS]_o = 1.6$ mM, T = 25°C, (**B**) $[MB]_o = 0.03$ mM (10 mg/L), [ACP] = 0.5 gr/L, [PMS] = 1.6 mM, T = 25°C.

result of experimental test illustrated that the higher concentration of PMS (5mM) can decrease the degradation rate of PMS/ACP-800 to oxidize dyes, because the residue of unreacted PMS could react with the $SO_4^{\bullet -}$ and produce the $SO_5^{\bullet -}$ ($SO_5^{\bullet -}/HSO_5^-$(1.1 V)) with less reactivity in comparison with $SO_4^{\bullet -}$ [79].

$$HSO_5^- + SO_4^{-\bullet} \rightarrow SO_5^{-\bullet} + SO_4^{2-} + H^+ \qquad (7)$$

3.3.4. Effect of pH

The pivotal influence of pH value on MO and MB degradation is shown in Figure 7. pK_a of MO and MB is 3.40 and 3.14, respectively. At pH 3.50 and 3.52, the optimal MO and MB degradation efficiency was obtained, respectively. Further increase of pH could decrease the removal rate of dye solution. The pH of the MO and MB solution has an effect on the degradation efficiency, because it changes the surface charge and the solubility of the dye. The degradation of MO on the PMS/ACP-800 system decreased as the pH increased from 3.50 to 9.40. It seems that the acidic condition is suitable for decolourization of MO for two reasons. Firstly, the surface of ACP-800 is ionized to carry a positive charge at low pH value. Therefore, due to the significant increase in the electrostatic interactions, the adsorption capacity increases for anionic MO dye. Secondly, MO dyes carry both positive and negative charges to produce an intermolecular salt, leading to the diminished hydration between MO and water molecules, and MO dyes are significantly adsorbed on the surface of the ACP-800. In addition, increasing pH would cause increased electrostatic repulsions between the negatively charged surface and the dye molecules, resulting in a decrease in degradation efficiency [80,81].

Similar to MO, the degradation of MB on the PMS/ACP-800 system decreased as the pH increased from 3.52 to 9.42, but the differences between degradation rates of mentioned pH values are less than those of MO . According to the obtained results and considering the MB as a cationic dye, it seems that adsorption mechanism on ACP take places via the following two paths. The first path is electrostatic force between MB that remained a negative charge on the adsorbent surface, considering the presence of repulsive forces between the solution media and the MB molecules which may derive the dye molecules towards the ACP surface. The second path is on-going via interaction between MB and aromatic rings in the ACP-activated carbon which led to more adsorption of MB on the ACP surface.

3.3.5. Effect of initial MO and MB concentration

The influence of initial concentration of MO and MB on the degradation percent in the PMS/ACP-800 system is investigated in Figure 6(G,H). These tests are evaluated by keeping 0.5 g/L ACP-800 dose, at pH = 3.5, 3 mM PMS dose and 1.5 h degradation time constant. ACP and PMS were added into 100 mL of the prepared dosage (5 to 25 ppm) of dye solution. The solution of 2.0 mL was pipetted out after desired time interval and filtered out. Then the concentrations of MO and MB were analysed immediately by maximum absorbance at wavelengths of 464 and 664 nm, respectively. This result confirms that the degradation rate of the dye from aqueous solution was found to decrease with increasing initial dye dose (Figure 6(G,H)).

3.4. TOC removal

TOC (Total Organic Carbon) analysis reflects mineralization of organic compounds. As depicted in Figure 8, the reduction levels of TOC for MO and MB at 1 h and 24 were 4.10 %, 31.00 %, 4.90% and 29.60%, respectively. It could be thought that mineralization stopped after 24 hrs.

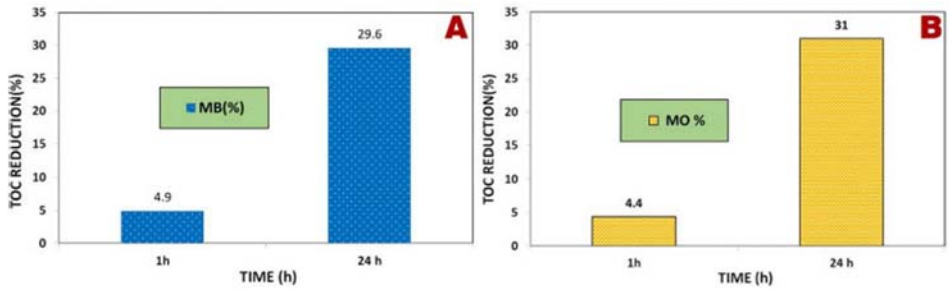

Figure 8. TOC reduction of (A) MB and (B) MO degradation in the ACP-800-PMS system, $[MB]_o = 0.03$ mM, $[MO]_o = 0.03$ mM, [ACP] = 0.5 gr/L, pH = 3.5, T = 25°C.

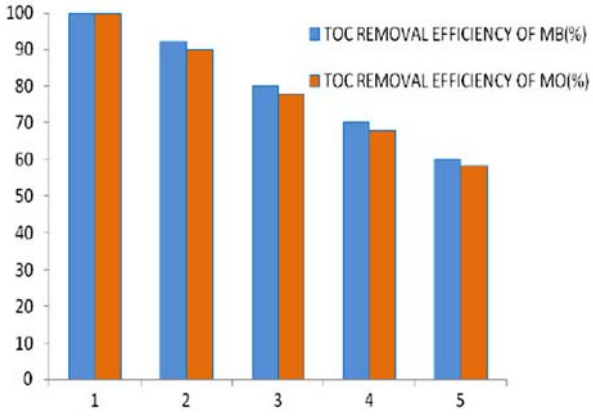

Figure 9. Reusability of MB and MO degradation in the ACP-800-PMS system, $[MB]_o = 0.03$ mM, $[MO]_o = 0.03$ mM, [ACP] = 0.5 gr/L, pH = 3.5, T = 25°C.

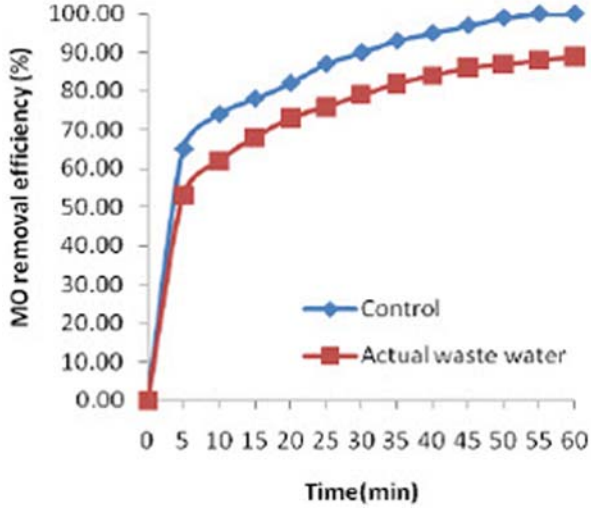

Figure 10. MO degradation in waste water media. $[MO]_o = 0.03$ mM (10 mg/L), $[ACP]_o = 0.5$ gr/L, $[PMS]_o = 3.0$ mM, T = 25°C.

The occurrence of mineralization of dyes showed that partial MO and MB was oxidized to carbon dioxide during the experiments [79].

3.5. Reusability of ACP-800

It is noted that carbonaceous materials may lose the activation capacity after a period of use related to the surface deactivation. The decreased catalytic ability of ACP-800 was probably ascribed to the block of adsorption and catalytic active sites by the intermediates formed during decolourization process [79]. As shown in Figure 9, reused experiments depicted that the ACP-800 catalyst has a good reusability with MO and MB efficiency after 3 cycles under optimal condition.

3.6. Effect of waste water media on MO degradation efficiency and method comparison

As shown in Figure 10, the MO degradation in the actual wastewater is monitored. The MO removal efficiency diminished to 89.0 % in comparison with control experiment. This demonstrated that wastewater components had a negative effect on the degradation of MO. The wastewater ingredients, such as organic compounds, can react with active radicals the same as $SO_4^{-\bullet}$ and $^{\bullet}OH$, which caused diminishing amounts of radicals reacting with MO, and as a result the dye degradation efficiency is reduced.

Table 3 summarizes the studies on the activation of PMS by the carbonaceous materials for the degradation of some contaminants.

As presented in Table 3, for the removal of the organic compounds, different performance was observed when using different carbonaceous materials as catalysts, which shows that different modified methods have different catalytic effects. Moreover, to attain the removal of organic contaminants, different amounts of catalyst and oxidants (PMS) were needed.

3.7. Identification of reactive radicals

To depict the degradation mechanism in detail, the involved $SO_4^{-\bullet}$ and $^{\bullet}OH$ during the degradation system were identified by radical trapping tests. Radical

Table 3. Carbon-based material-activated PMS for the degradation of the contaminants.

Pollutant	Source water	Pollutant concentration	PMS concentration	Carbon-based material	pH	Reaction time(h)	Degradation (%)	Reference
Methyl Orange, Methylene Blue	Deionized water and Waste water	25 mgL^{-1}	3 mM	ACP-800(1+2), 0.5 gL^{-1}	3.50	1.5	100	This Study
Orange G	Waste water	44 μM 20 mgL^{-1}	1.76	Activated carbon fibre, 0.3 gL^{-1}	7.0	0.83	100	[88]
Phenol	Ultrapure water	20 mgL^{-1}	2 gL^{-1}	N-modified carbon nanotube 0.2 gL^{-1}	6.5	4	100	[89]
Azo dye (AO7)	Deionized water	57 μM 20 mgL^{-1}	1.14 mM	Carbon nanotube 0.1 gL^{-1}	7	0.83	100	[90]
Triclosan	Water and waste water	10 mgL^{-1}	0.8 mM	Sludge-derived biochar 1.0 gL^{-1}	7.2	2	100	[79]

quenching tests were performed using ETOH and TBA (t-butyl alcohol), respectively. Actually, alcohol makes challenges with the organic compound to react with the radical species so that the degradation rate is awaited to be decreased.

A considerably inhibition event was occurred when ETOH was added to the degradation system as a α-hydrogen-containing alcohol.

ETOH is scavenging both radicals ($SO_4^{-\bullet}$ and $^{\bullet}OH$) (($K_{ETOH-^{\bullet}OH} = (1.8–2.8) \times 10^9\ M^{-1}\ S^{-1}$, $K_{ETOH\ -\ SO4-^{\bullet}} = (1.6–7.7) \times 10^7\ M^{-1}\ S^{-1}$)), while TBA is the scavenger of $^{\bullet}OH$ because TBA does not contain α-hydrogen and has a much higher tendency to scavenge hydroxyl radical (($K_{TBA-^{\bullet}OH} = (3.8\text{-}7.6) \times 10^8\ M^{-1}\ S^{-1}$, $K_{TBA\ -\ SO4-^{\bullet}} = (4.0–9.1) \times 10^5\ M^{-1}\ S^{-1}$)) [74,82]. The presence of 1.0 M ETOH caused significant suppression in the oxidation process, with the decolourization efficiency diminishing from 89%, 90% to 35 %, 37 % for MO and MB, respectively. For TBA-added test, the presence of 1.0 M TBA suppressed the oxidation process with the decolourization efficiency diminishing from 89%, 90% to 76%,77 %, respectively. So, the efficiency decreasing rate of ETOH and TBA systems is (54% for MO, 53% for MB) and (13% for MO, 13% for MB), respectively.

On the other hand, sulphate radicals are the main active species at acid condition that are strong oxidants with high oxidation potential (2.5–3.1 V) that can be produced by breaking the peroxo-bond of PMS during the experiment. Also sulphate radical has a higher half-life time than hydroxyl radical (30–40 μs vs 20 ns) considerably due to its ability to react with organic species during electron transfer, while hydroxyl radical acts randomly and takes part in different reactions with the same tendency [74].

According to the results, both $SO_4^{-\bullet}$ and $^{\bullet}OH$ have their effect in the degradation process but due to the notable difference between the efficiency diminishing rates sulphate radicals are the primary reactive species at acid condition [74], so $SO_4^{-\bullet}$ plays an essential role in the ACP-800-PMS system (Figure 11).

3.8. Degradation mechanism

By the PMS/ACP-800 system, the colour of the dye solution is gradually faded as the reaction proceeded, which indicates that the MO concentration decreased obviously. According to the previous work and experimental tests, the degradation intermediates produced in the ACP-800-PMS system at different times were

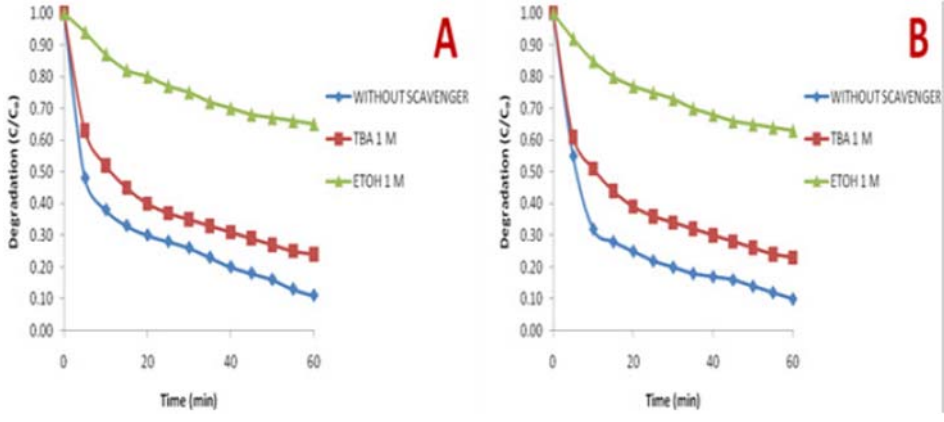

Figure 11. Effect of scavenger on MO and MB degradation; (**A**) $[MO]_o$ = 0.03 mM, [ACP] = 0.5 gr/L,[PMS] = 3 mM, T = 25°C, (**B**) $[MB]_o$ = 0.03 mM, [ACP] = 0.5 gr/L, [PMS] = 3 mM, T = 25°C.

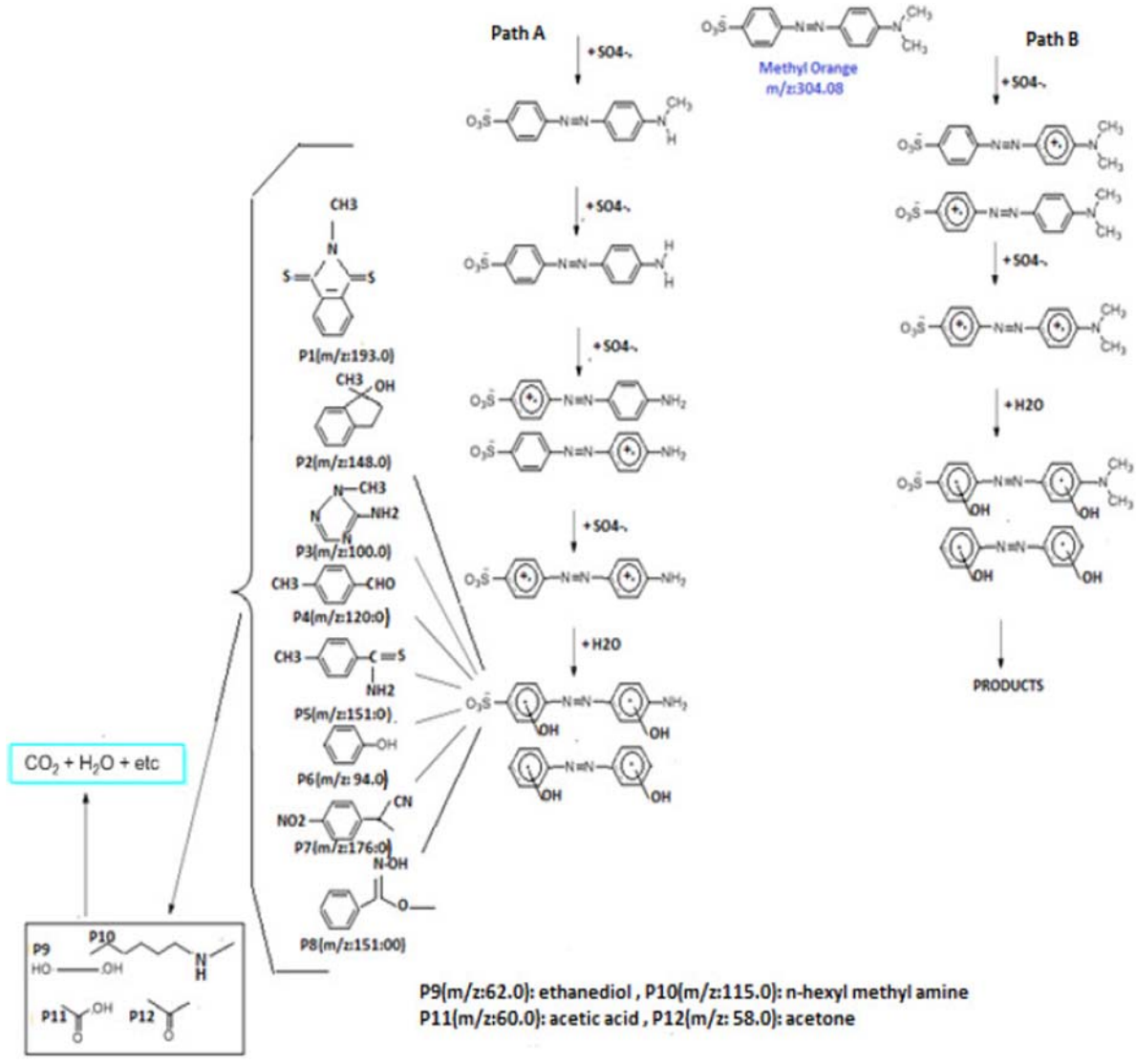

Scheme 1. Plausible degradation mechanism of MO by the ACP-800-PMS system.

identified by GC-MS technologies [83,84]. To propose the possible degradation mechanism, the molecular structure of possible intermediates is shown in Scheme 1. The main peak of MO dye was no longer observed after 60 min of process, indicating the MO was totally degraded. Other new peaks corresponded to the intermediate compounds in the degradation of MO.

Three principal mechanisms have been suggested for the first step of $SO_4^{-\bullet}$ oxidation of aromatic compounds: radical adduct formation, hydrogen atom abstraction and single electron transfer (SET) [85]. According to the GC/MS data of this work and previous studies, the SET pathway is the major reaction mechanism for the conversion of aromatic compound which may happen from the aromatic ring and produce a phenyl radical cation. In general, this radical cation can react with the water to adding a hydroxyl group to the ring [85]. By this explanation, Scheme 1 is suggested as the MO degradation mechanism. The TIC and MS spectra of MO degradation main products are presented in Figures 12 and 13.

The peaks with *m/z* = 193.0 (**P1**), 148.0 (**P2**),100.0 (**P3**), 120.0 (**P4**), 151.0 (**P5**), 94.0 (**P6**), 176.0 (**P7**), 151.0 (**P8**),62.0 (**P9**), 115.0 (**P10**),60.0(**P11**) and 58.0 (**P12**) were identified (Scheme 1). In the path A, the N–C with the lowest bond energy is first broken and loss of methyl groups. Much short lifetime of radical cations (0.1-1μs) produced in SET reactions [85] makes it difficult to detect these reaction intermediates in the GC/MS diagram.

In the MB degradation system (Scheme 2), the intermediates were basically produced through loss of functional group, dechlorination (**P13)**, N-desulfurization (**P14),** N-demethylation (**P19**) and ring-opening reactions (**P15-21**) by radicals [86,87]. PMS was catalysed to decompose and sulphate/hydroxyl radicals

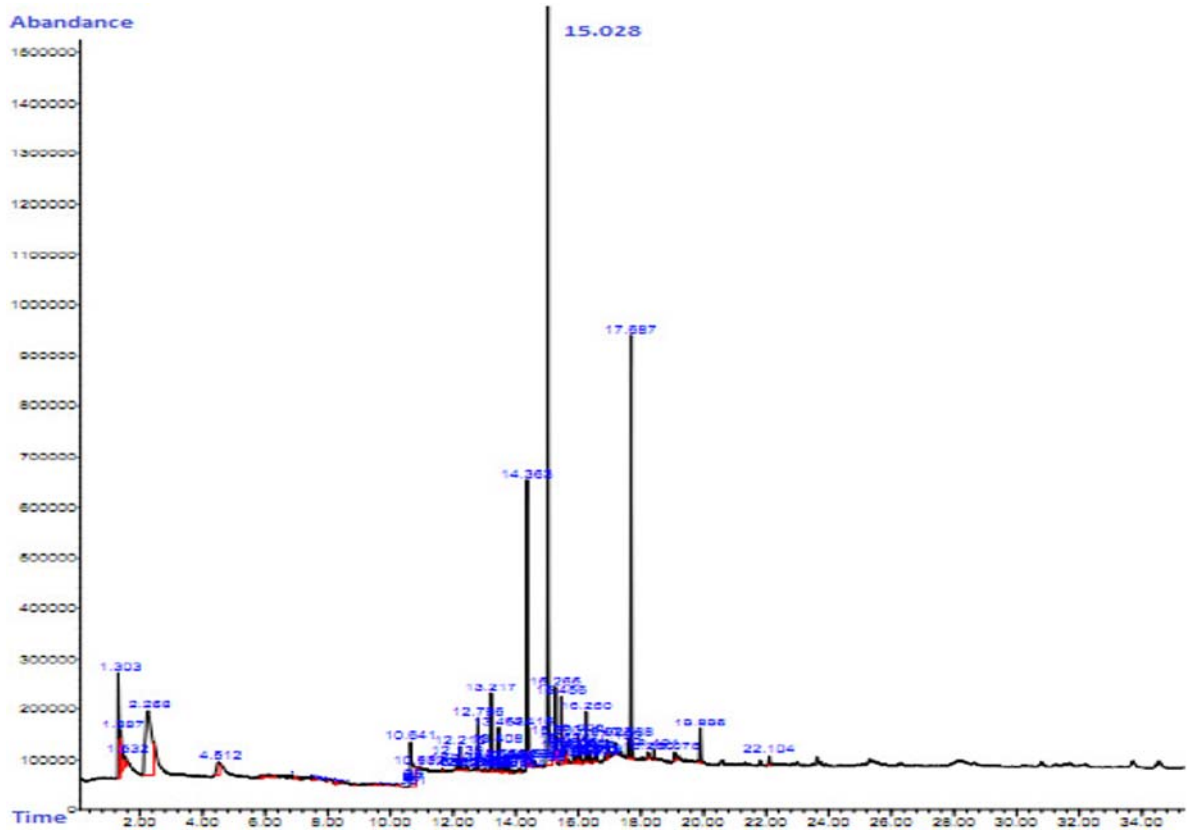

Figure 12. TIC of MO degradation main products.

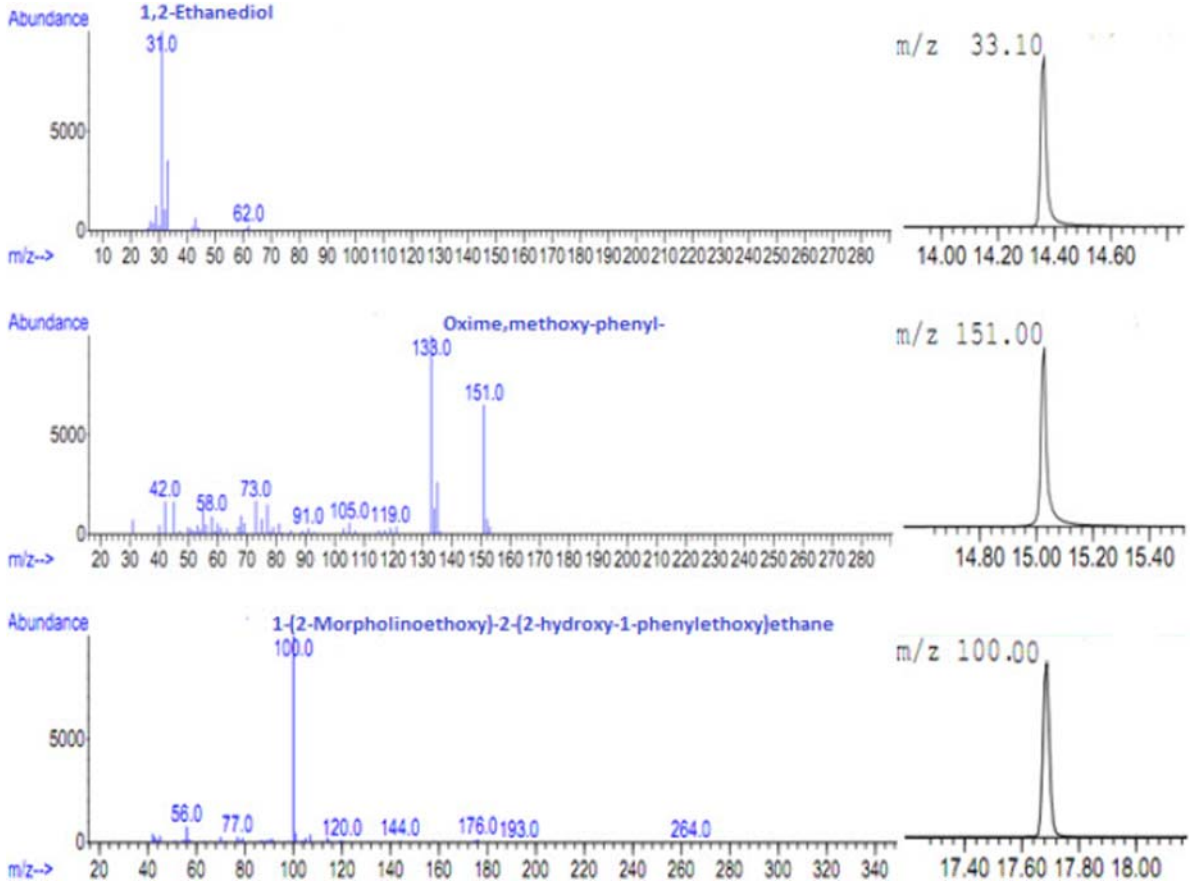

Figure 13. MS spectra of MO degradation main products.

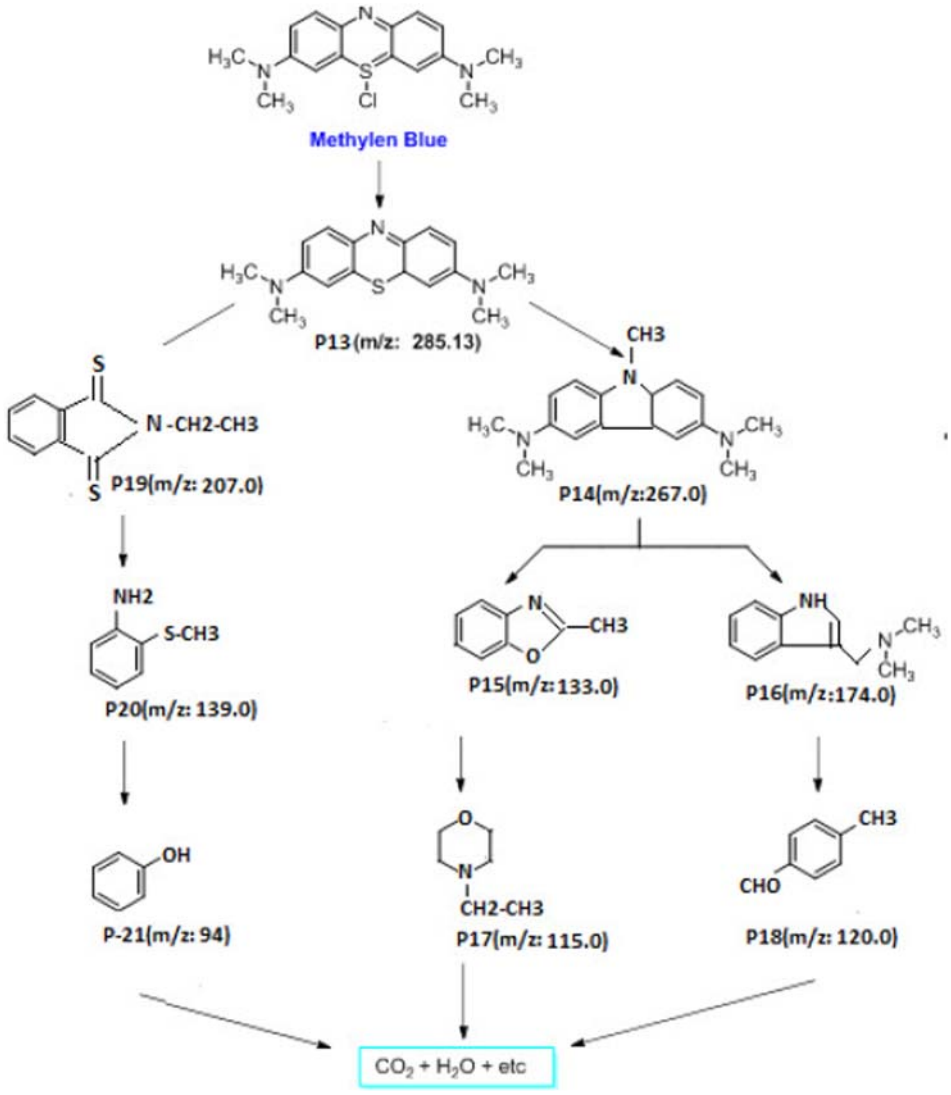

Scheme 2. Plausible degradation mechanism of MB by the ACP-800-PMS system.

were generated on the surface of the ACP-800 and then transferred to the liquid phase to decompose MB in solution. The peaks with $m/z = 267.0$ (**P14**),133.0(**P15**), 174.0(**P16**), 115.0 (**P17**), 120.0 (**P18**), 207.0 (**P19**), 139.0 **(P20)** and 94.0 (**P21**) were detected by GC/MS. In the final step of degradation of MB, the opening ring products, such as glycerin, ethylene glycol, acetic acid and formic acid, transformed into inorganic ions.

4. Conclusion

The potential to use waste as an alternative source was demonstrated, giving rise to an environment-friendly material with a lower cost of production. Therefore, this work was conducted to investigate the potential use of ACP-800 as a native activator to degradation of MB and MO dye from wastewater effluents. The findings disclosed that the amount of ACP-800, dye and oxidant concentration, initial pH level and temperature significantly affected dye degradation efficiency. Reusability investigation confirmed that ACP-800 (1+2) could be applied frequently for the degradation dye from the contaminated solution. Above all, it seems pertinent to note that the experimental data highlighted that ACP-800 could be utilized as a promising activator for the degradation of MB and MO dyes from wastewater since the pistachio shells are comfortably and economically available in large quantities.

Disclosure statement

No potential conflict of interest was reported by the author(s).

Funding

This work was supported by the University of Kashan under [grant number 463609].

ORCID

Ali Gholami http://orcid.org/0000-0002-9145-9815
Fakhreddin Mousavinia http://orcid.org/0000-0002-3745-807X

References

[1] Chatterjee MJ, Ahamed SKT, Mitra M, et al. Visible-light influenced photocatalytic activity of polyaniline -bismuth selenide composites for the degradation of methyl orange, rhodamine B and malachite green dyes. Appl Surf Sci. 2019;470:472–483.
[2] Asfaram A, Ghaedi M, Ahmadi AMH, et al. Ultrasound-assisted binary adsorption of dyes onto Mn@ CuS/ZnS-NC-AC as a novel adsorbent: application of chemometrics for optimization and modeling. J Ind Eng Chem. 2017;54:377–388.
[3] Mazaheri H, Ghaedi M, Ahmadi Azqhandi MH, et al. Application of machine/statistical learning, artificial intelligence and statistical experimental design for the modeling and optimization of methylene blue and Cd (II) removal from a binary aqueous solution by natural walnut carbon. Phys Chem Chem Phys. 2017;19 (18):11299–11317.
[4] Yu F, Cao L, Huang J, et al. Effects of pH on the microstructures and optical property of FeWO4 nanocrystallites prepared via hydrothermal method. Ceram Int. 2013;39 (4):4133–4138.
[5] Nasuha N, Hameed B. Adsorption of methylene blue from aqueous solution onto NaOH-modified rejected tea. Chem Eng J. 2011;166(2):783–786.
[6] Holkar CR, Jadhav AJ, Pinjari DV, et al. A critical review on textile wastewater treatments: possible approaches. J Environ Manage. 2016;182:351–366.
[7] Yang H, Yuan H, Hu Q, et al. Synthesis of mesoporous C/MoS2 for adsorption of methyl orange and photo-catalytic sterilization. Appl Surf Sci. 2020;504:144445.
[8] Wang H, Xie R, Zhang J, et al. Preparation and characterization of distillers' grain based activated carbon as low cost methylene blue adsorbent: mass transfer and equilibrium modeling. Adv Powder Technol. 2018;29(1):27–35.
[9] Wang Q, Lei X, Pan F, et al. A new type of activated carbon fibre supported titanate nanotubes for high-capacity adsorption and degradation of methylene blue. Colloids Surf, A. 2018;555:605–614.
[10] Han Q, Wang J, Goodman BA, et al. High adsorption of methylene blue by activated carbon prepared from phosphoric acid treated eucalyptus residue. Powder Technol. 2020;366:239–248.
[11] Danish M, Ahmad T, Hashim R, et al. Comparison of surface properties of wood biomass activated carbons and their application against rhodamine B and methylene blue dye. Surf Interfaces. 2018;11:1–13.
[12] Bedin KC, Martins AC, Cazetta AL, et al. KOH-activated carbon prepared from sucrose spherical carbon: adsorption equilibrium, kinetic and thermodynamic studies for Methylene Blue removal. Chem Eng J. 2016;286:476–484.
[13] Hu C, Shen J-J, Chang A-L, et al. Microwave plasma torch synthesis of Zn Al oxides as adsorbent and photocatalyst for organic compounds removal. Powder Technol. 2019;344:454–462.
[14] Labiadh L, Kamali AR. Textural, structural and morphological evolution of mesoporous 3D graphene saturated with methyl orange dye during thermal regeneration. Diam Relat Mater. 2020;103:107698.
[15] Zhang YX, Hao XD, Kuang M, et al. Preparation, characterization and dye adsorption of Au nanoparticles/ZnAl layered double oxides nanocomposites. Appl Surf Sci. 2013;283:505–512.
[16] Kono H, Kusumoto R. Removal of anionic dyes in aqueous solution by flocculation with cellulose ampholytes. J Water Process Eng. 2015;7:83–93.
[17] Morshedi D, Mohammadi Z, Akbar Boojar MM, et al. Using protein nanofibrils to remove azo dyes from aqueous solution by the coagulation process. Colloids Surf B. 2013;112:245–254.
[18] Lin SH, Lin CM. Treatment of textile waste effluents by ozonation and chemical coagulation. Water Res. 1993;27(12):1743–1748.
[19] Xu Y, Lebrun RE., Gallo P-J, et al. Treatment of textile dye plant effluent by nanofiltration membrane. Sep Sci Technol. 1999;34(13):2501–2519.
[20] Ren Y, Zhang W, Wang S, et al. MIL-PVDF blend ultrafiltration membranes with ultrahigh MOF loading for simultaneous adsorption and catalytic oxidation of methylene blue. J Hazard Mater. 2019;365:312–321.
[21] Yao L, Zhang L, Wang R, et al. A new integrated approach for dye removal from wastewater by polyoxometalates functionalized membranes. J Hazard Mater. 2016;301:462–470.
[22] Ahn D-H, Chang W-S, Yoon T-I. Dyestuff wastewater treatment using chemical oxidation, physical adsorption and fixed bed biofilm process. Process Biochem. 1999;34 (5):429–439.
[23] Qi J, Li X, Zheng H, et al. Simultaneous removal of methylene blue and copper(II) ions by photoelectron catalytic oxidation using stannic oxide modified iron(III) oxide composite electrodes. J Hazard Mater. 2015;293:105–111.
[24] Wolski L, Ziolek M. Insight into pathways of methylene blue degradation with H2O2 over mono and bimetallic Nb, Zn oxides. Appl Catal, B. 2018;224:634–647.
[25] Dou R, Cheng H, Ma J, et al. Catalytic degradation of methylene blue through activation of bisulfite with CoO nanoparticles. Sep Purif Technol. 2020;239:116561.
[26] Nguyen TB, Doong R-A, Huang CP, et al. Activation of persulfate by CoO nanoparticles loaded on 3D mesoporous carbon nitride (CoO@meso-CN) for the degradation of methylene blue (MB). Sci Total Environ. 2019;675:531–541.
[27] Xin Zhang Y, Long Guo X, Huang M, et al. Engineering birnessite-type MnO2 nanosheets on fiberglass for pH-dependent degradation of methylene blue. J Phys Chem Solids. 2015;83:40–46.
[28] Huang J, Dai Y, Singewald K, et al. Effects of MnO2 of different structures on activation of peroxymonosulfate for bisphenol A degradation under acidic conditions. Chem Eng J. 2019;370:906–915.
[29] Wang S, Wang J. Oxidative removal of carbamazepine by peroxymonosulfate (PMS) combined to ionizing radiation: degradation, mineralization and biological toxicity. Sci Total Environ. 2019;658:1367–1374.
[30] Jia Z, Chen Q, Li C, et al. Facile in situ preparation of fibrous Ag/AgCl composites with efficient photocatalytic

degradation of methyl orange under solar light. J Phys Chem Solids. 2020;140:109360.
[31] Tao X, Yang C, Huang L, et al. Novel plasma assisted preparation of ZnCuFeCr layered double hydroxides with improved photocatalytic performance of methyl orange degradation. Appl Surf Sci. 2020;507:145053.
[32] Narendhran S, Shakila PB, Manikandan M, et al. Spectroscopic investigation on photocatalytic degradation of methyl orange using Fe2O3/WO3/FeWO4 nanomaterials. Spectrochim Acta Part A. 2020;232:118164.
[33] Wen D, Li W, Lv J, et al. Methylene blue degradation by the VUV/UV/persulfate process: effect of pH on the roles of photolysis and oxidation. J Hazard Mater. 2020;391:121855.
[34] Gottam R, Srinivasan P, La DD, et al. Improving the photocatalytic activity of polyaniline and a porphyrin *via* oxidation to obtain a salt and a charge-transfer complex. New J Chem. 2017;41(23):14595–14601.
[35] Umamaheswari C, Lakshmanan A, Nagarajan N. Green synthesis, characterization and catalytic degradation studies of gold nanoparticles against Congo red and methyl orange. J Photochem Photobiol, B. 2018;178:33–39.
[36] Li M, Qiang Z, Hou P, et al. VUV/UV/chlorine as an enhanced advanced oxidation process for organic pollutant removal from water: assessment with a novel minifluidic VUV/UV photoreaction system (MVPS). Environ Sci Technol. 2016;50(11):5849–5856.
[37] Yong K, Wang Z-l, Wang Y, et al. Degradation of methyl orange in artificial wastewater through electrochemical oxidation using exfoliated graphite electrode. New Carbon Mater. 2011;26(6):459–464.
[38] Khuntia S, Majumder SK, Ghosh P. Catalytic ozonation of dye in a microbubble system: hydroxyl radical contribution and effect of salt. J Env Chem Eng. 2016;4(2):2250–2258.
[39] Ren B, Miao J, Xu Y, et al. A grape-like N-doped carbon/CuO-Fe2O3 nanocomposite as a highly active heterogeneous fenton-like catalyst in methylene blue degradation. J Clean Prod. 2019;240:118143.
[40] Innocenzi V, Prisciandaro M, Centofanti M, et al. Comparison of performances of hydrodynamic cavitation in combined treatments based on hybrid induced advanced Fenton process for degradation of azo-dyes. J Env Chem Eng. 2019;7(3):103171.
[41] Omri A, Hamza W, Benzina M. Photo-Fenton oxidation and mineralization of methyl orange using Fe-sand as effective heterogeneous catalyst. J Photochem Photobiol A. 2020;393:112444.
[42] Wang J, Wang S. Activation of persulfate (PS) and peroxymonosulfate (PMS) and application for the degradation of emerging contaminants. Chem Eng J. 2018;334:1502–1517.
[43] Cai B, Feng J-f, Peng Q-y, et al. Super-fast degradation of high concentration methyl orange over bifunctional catalyst Fe/Fe3C@C with microwave irradiation. J Hazard Mater. 2020;392:122279.
[44] Wang C, Shi Z-h, Peng L, et al. Preparation of carbon foam-loaded nano-TiO2 photocatalyst and its degradation on methyl orange. Surf Interfaces. 2017;7:116–124.
[45] Zeng L, Zhe F, Wang Y, et al. Preparation of interstitial carbon doped BiOI for enhanced performance in photocatalytic nitrogen fixation and methyl orange degradation. J Colloid Interface Sci. 2019;539:563–574.
[46] Zhong Y, Chen R, Rojas-Sossa J-P, et al. Anaerobic co-digestion of energy crop and agricultural wastes to prepare uniform-format cellulosic feedstock for biorefining. Renew Energy. 2020;147:1358–1370.
[47] Yang S-S, Chen Y-d, Zhang Y, et al. A novel clean production approach to utilize crop waste residues as co-diet for mealworm (tenebrio molitor) biomass production with biochar as byproduct for heavy metal removal. Environ Pollut. 2019;252:1142–1153.
[48] Momayez F, Karimi K, Taherzadeh MJ. Energy recovery from industrial crop wastes by dry anaerobic digestion: A review. Ind Crops Prod. 2019;129:673–687.
[49] Statistical yearbook for nuts and dried fruits (2017–2018). [cited 2018 Oct. 23]. http://www.nutfruit.org/files/tech/1523960263_INC_Statistical_Yearbook_2017_2018.pdf.
[50] Hamed M, Bougatef H, Karoud W, et al. Polysaccharides extracted from pistachio external hull: characterization, antioxidant activity and potential application on meat as preservative. Ind Crops Prod. 2020;148:112315.
[51] Taghizadeh-Alisaraei A, Assar HA, Ghobadian B, et al. Potential of biofuel production from pistachio waste in Iran. Renew Sustain Energy Rev. 2017;72:510–522.
[52] Banerjee M, Basu RK, Das SK. Adsorptive removal of Cu(II) by pistachio shell: isotherm study, kinetic modelling and scale-up designing – continuous mode. Environ Technol Innov. 2019;15:100419.
[53] Kasiri N, Fathi M. Production of cellulose nanocrystals from pistachio shells and their application for stabilizing Pickering emulsions. Int J Biol Macromol. 2018;106:1023–1031.
[54] Younes A, Ali JS, Nur MT, et al. Pistachio shells as remediating agents for uranium in contaminated industrial seawater. J Environ Radioact. 2020;217:106209.
[55] Şahin Ö, Yardim Y, Baytar O, et al. Enhanced electrochemical double-layer capacitive performance with CO2 plasma treatment on activated carbon prepared from pyrolysis of pistachio shells. Int J Hydrogen Energy. 2020;45(15):8843–8852.
[56] Akl M, Mostafa M, Bashanaini M. Enhanced removal of some cationic dyes from environmental samples using sulphuric acid modified pistachio shells derived activated carbon. J Chromatogr Sep Tech. 2016;7:4.
[57] Sevilla M, Ferrero GA, Fuertes AB. Beyond KOH activation for the synthesis of superactivated carbons from hydrochar. Carbon NY. 2017;114:50–58.
[58] Staciwa P, Narkiewicz U, Sibera D, et al. Carbon spheres as CO2 sorbents. Appl Sci. 2019;9(16):3349.
[59] Lee JH, Park SJ. Potassium oxalate as an alternative activating reagent of corn starch-derived porous carbons for methane storage. J Nanosci Nanotechnol. 2020;20(11):7124–7129.
[60] Kaghazchi T, Kolur NA, Soleimani M. Licorice residue and pistachio-nut shell mixture: a promising precursor for activated carbon. J Ind Eng Chem. 2010;16(3):368–374.
[61] Komnitsas K, Zaharaki D, Pyliotis I, et al. Assessment of pistachio shell biochar quality and Its potential for adsorption of heavy metals. Waste Biomass Valorization. 2015;6(5):805–816.

[62] Yang T, Lua AC. Characteristics of activated carbons prepared from pistachio-nut shells by potassium hydroxide activation. Microporous Mesoporous Mater. 2003;63:113–124.
[63] Ahmadpour A, Do D. The preparation of activated carbon from macadamia nutshell by chemical activation. Carbon NY. 1997;35(12):1723–1732.
[64] Yaman S. Pyrolysis of biomass to produce fuels and chemical feedstocks. Energy Convers Manage. 2004;45 (5):651–671.
[65] Liu Z, Quek A, Kent Hoekman S, et al. Production of solid biochar fuel from waste biomass by hydrothermal carbonization. Fuel. 2013;103:943–949.
[66] Cao X, Harris W. Properties of dairy-manure-derived biochar pertinent to its potential use in remediation. Bioresour Technol. 2010;101:5222–5228.
[67] Sharma RK, Wooten JB, Baliga VL, et al. Characterization of chars from pyrolysis of lignin. Fuel. 2004;83:1469–1482.
[68] Pastorova I, Botto RE., Arisz PW, et al. Cellulose char structure: a combined analytical Py-GC-MS, FTIR, and NMR study. Carbohydr Res. 1994;262:27–47.
[69] Chen B, Chen Z, Lv S. A novel magnetic biochar efficiently sorbs organic pollutants and phosphate. Bioresour Technol. 2011;102(2):716–723.
[70] Çağlar A, Demirbaş A. Conversion of cotton cocoon shell to liquid products by pyrolysis. Energy Convers Manage. 2000;41(16):1749–1756.
[71] Hossain MK, Strezov V, Chan KY, et al. Influence of pyrolysis temperature on production and nutrient properties of wastewater sludge biochar. J Environ Manage. 2011;92(1):223–228.
[72] Angın D, Köse T, Selengil U. Production and characterization of activated carbon prepared from safflower seed cake biochar and its ability to absorb reactive dyestuff. Appl Surf Sci. 2013;280:705–710.
[73] Glaser B, Haumaier L, Guggenberger G, et al. The 'Terra preta' phenomenon: a model for sustainable agriculture in the humid tropics. Naturwissenschaften. 2001;88:37–41.
[74] Ghanbari F, Moradi M. Application of peroxymonosulfate and its activation methods for degradation of environmental organic pollutants: review. Chem Eng J. 2017;310:41–62.
[75] Waldemer RH, Tratnyek PG, Johnson RL, et al. Oxidation of chlorinated ethenes by heat-activated persulfate: kinetics and products. Environ Sci Technol. 2007;41 (3):1010–1015.
[76] Hori H, Nagaoka Y, Murayama M, et al. Efficient decomposition of perfluorocarboxylic acids and alternative fluorochemical surfactants in hot water. Environ Sci Technol. 2008;42(19):7438–7443.
[77] Zrinyi N, Pham AL-T. Oxidation of benzoic acid by heat-activated persulfate: effect of temperature on transformation pathway and product distribution. Water Res. 2017;120:43–51.
[78] Zhang Q, Cheng S, Xia H, et al. Paracetamol degradation performance and mechanisms using microwave-assisted heat-activated persulfate in solutions. Water Air Soil Pollut. 2019;230(12):271.
[79] Wang S, Wang J. Activation of peroxymonosulfate by sludge-derived biochar for the degradation of triclosan in water and wastewater. Chem Eng J. 2019;356:350–358.
[80] Hu Lv, Zhang G, Liu M, et al. Enhanced degradation of Bisphenol A (BPA) by peroxymonosulfate with Co3O4-Bi2O3 catalyst activation: effects of pH, inorganic anions, and water matrix. Chem Eng J. 2018;338:300–310.
[81] Sun B, Yuan Y, Li H, et al. Waste-cellulose-derived porous carbon adsorbents for methyl orange removal. Chem Eng J. 2019;371:55–63.
[82] Li G,, Zhong Z, Yang C et al. Degradation of acid orange 7 by peroxymonosulfate activated by cupric oxide. J Water Supply: Res Technol-Aqua. 2019;68(1):29–38.
[83] Du L, Wu J, Qin S, et al. Degradation mechanism of methyl orange by electrochemical process on RuOx–PdO/Ti electrode. Water Sci Technol. 2011;63(7):1539–1545.
[84] Du L-N, Li G, Zhao Y-H, et al. Efficient metabolism of the azo dye methyl orange by *Aeromonas* sp. strain DH-6: characteristics and partial mechanism. Int Biodeterior Biodegradation. 2015;105:66–72.
[85] Luo S, Wei Z, Dionysiou DD, et al. Mechanistic insight into reactivity of sulfate radical with aromatic contaminants through single-electron transfer pathway. Chem Eng J. 2017;327:1056–1065.
[86] Huang F, Chen L, Wang H, et al. Analysis of the degradation mechanism of methylene blue by atmospheric pressure dielectric barrier discharge plasma. Chem Eng J. 2010;162(1):250–256.
[87] Wang Q, Tian S, Ning P. Degradation mechanism of methylene blue in a heterogeneous fenton-like reaction catalyzed by ferrocene. Ind Eng Chem Res. 2014;53 (2):643–649.
[88] Chen J, Hong W, Huang T, et al. Activated carbon fiber for heterogeneous activation of persulfate: implication for the decolorization of azo dye. Environ Sci Pollut Res Int. 2016;23(18):18564–18574.
[89] Sun H, Kwan CK, Suvorova A, et al. Catalytic oxidation of organic pollutants on pristine and surface nitrogen-modified carbon nanotubes with sulfate radicals. Appl Catal, B. 2014;154-155:134–141.
[90] Chen J, Zhang L, Huang T, et al. Decolorization of azo dye by peroxymonosulfate activated by carbon nanotube: radical versus non-radical mechanism. J Hazard Mater. 2016;320:571–580.